A safeguards approach for molten salt reactors: Direct gamma-spectrometry of ^{233}U

Jonathan L. Burnett

Pacific Northwest National Laboratory, PO Box 999, Richland, WA, USA

ARTICLE INFO

Keywords:
Uranium-233
Gamma-spectrometry
Safeguards
Molten salt reactor

ABSTRACT

Multidimensional gamma-spectrometry is a potential solution for safeguarding future thorium-fuelled molten salt reactors (MSRs). A high-sensitivity system developed at Pacific Northwest National Laboratory (PNNL), the Advanced Radionuclide Gamma spectrometer (ARGO), has demonstrated direct ^{233}U assay in freshly irradiated fuel salt samples using a dual-detector configuration and the 97.1 keV gamma-emission. These measurements were made using 1.4×10^6 Bq of ^{233}U activity (at 1.4×10^8 fissions), at relatively high dead times (10.4%), and using short count durations of ~800 s. Other major emissions were also evaluated (42.5 keV, 54.7 keV, 146.4 keV), in additional to limited (1.96%) Compton suppression, but provided less consistent determination of the ^{233}U activity. Accurate ^{233}U measurement was also demonstrated using its four-coincidence gamma-emissions (42.5 keV, 54.7 keV; 42.5 keV, 278.1 keV; 146.4 keV, 174.2 keV; 146.4 keV, 219 keV). Further improvements in coincidence measurements may be achievable with improvements in the detector configuration and nuclear data. Whilst this demonstration utilized the ARGO laboratory system, a similar dual-detector configuration could be utilized for online safeguards measurements.

1. Introduction

Molten salt reactors (MSRs) are a nuclear reactor design that utilize a molten salt mixture as the primary reactor coolant. In some designs, the reactor fuel is also dissolved in the coolant. The concept was originally demonstrated as part of the Aircraft Reactor Experiment (ARE) during 1954 [1–3], and Molten Salt Reactor Experiment (MSRE) from 1965–1969 [4,5]. There has been renewed interest in this concept by the USA, Russia, China, France and Japan, and the selection of MSRs as a Generation IV reactor design [6]. Much of the interest relates to using thorium (^{232}Th) to breed fissile uranium (^{233}U), for which safeguards technology is being developed [7]. As defined by the International Atomic Energy Agency (IAEA), an objective of safeguards is the timely detection of the diversion of significant quantities of nuclear material that could be used for illicit purposes [8]. Non-destructive analysis (NDA) techniques are commonly used for this purpose, but for ^{233}U the technology readiness level (TRL) needs to increase further, as ^{233}U is subject to the same safeguard protocols as ^{239}Pu [9]. For an MSR, difficulties include the low ^{233}U gamma-emission (0.072% at 42.4 keV), interferences from fission and activation products (e.g., ^{140}La and ^{24}Na), and how to perform measurement under high temperature and corrosivity.

Next-generation multidimensional gamma-spectrometry systems have the potential for extremely high-sensitivity radionuclide analysis and may be suitable for direct ^{233}U measurement [10]. Within the Shallow Underground Laboratory (SUL) at the Pacific Northwest National Laboratory (PNNL, USA), the Advanced Radionuclide Gamma-spectrOmeter (ARGO) system has been developed [11]. The ARGO is comprised of two Broad Energy Germanium (BEGe) detectors aligned in an up–down configuration. The multi-detector near 4π configuration, combined with a versatile multichannel analyzer (MCA) [12], enables the simultaneous detection of single, combined, Compton suppressed [13–15] and coincidence measurements [16–18]. In previous work [11], the ARGO has demonstrated order of magnitude sensitivity improvements for fission products in irradiated ^{235}U and ^{238}U samples compared to conventional single-detector gamma-spectrometry systems. This effort applies the capabilities of the ARGO to the direct determination of ^{233}U in freshly irradiated samples, including those containing potassium chloride (KCl) and sodium chloride (NaCl), which could be considered representative of fuel salt samples from next-generation MSRs. This also includes the accurate measurement of ^{233}U using some of its coincidence gamma-emissions, which has not been previously demonstrated.

2. ^{233}U

A thorium MSR utilizes a fuel salt such as ThF_4 or $ThCl_4$, and the breeding of ^{233}U is achievable using slow and fast neutrons with relatively high efficiency. It occurs through the neutron irradiation of naturally occurring ^{232}Th ($t_{1/2} = 1.40 \times 10^{10}$ y) and the capture reaction $^{232}Th(n, \gamma)^{233}Th$. The ^{233}Th ($t_{1/2} = 24$ m) then successively

E-mail address: jonathan.burnett@pnnl.gov.

Table 1
The most abundant X-ray and gamma-emissions energies for ^{233}U. For gamma-spectrometry measurement it is practical to combine the 42.43 keV and 42.63 keV emissions. The nuclear data is from the Evaluated Nuclear Data File (ENDF VIII.0) database [20].

Energy (keV)	Probability	Type	Energy (keV)	Probability	Type
16.10 ± 2.44	2.4E−02 ± 3.7E−3	X-ray	29.19 ± 0.20	7.8E−05 ± 5.0E−6	γ-ray
12.96 ± 1.91	2.3E−02 ± 3.5E−3	X-ray	317.17 ± 0.002	7.4E−05 ± 4.1E−6	γ-ray
3.06 ± 0.39	8.9E−03 ± 1.2E−3	X-ray	146.35 ± 0.0006	6.5E−05 ± 3.0E−6	γ-ray
19.25 ± 2.88	5.4E−03 ± 8.2E−4	X-ray	89.96 ± 0.0002	6.0E−05 ± 6.3E−6	X-ray
12.73 ± 1.16	3.2E−03 ± 2.9E−4	X-ray	164.52 ± 0.0005	6.0E−05 ± 3.0E−6	γ-ray
42.43 ± 0.20	7.2E−04 ± 5.0E−7	γ-ray	291.36 ± 0.009	5.3E−05 ± 3.5E−6	γ-ray
97.13 ± 0.0003	2.0E−04 ± 1.0E−5	γ-ray	118.97 ± 0.005	3.6E−05 ± 1.8E−6	γ-ray
54.70 ± 0.001	1.7E−04 ± 8.0E−6	γ-ray	245.35 ± 0.001	3.6E−05 ± 1.8E−6	γ-ray
42.63 ± 0.0002	1.3E−04 ± 4.0E−5	γ-ray	53.61 ± 0.001	3.5E−05 ± 1.8E−6	γ-ray
93.35 ± 0.0003	9.9E−05 ± 1.0E−5	X-ray	217.15 ± 0.004	3.3E−05 ± 1.6E−6	γ-ray

beta-decays to form ^{233}Pa ($t_{1/2}$ = 2.4 d) and then fissile ^{233}U ($t_{1/2}$ = 1.59×10^5 y). During this process, non-fissile ^{232}U ($t_{1/2}$ = 68.9 y) may be produced as the intermediary ^{233}Pa may undergo the reaction ^{233}Pa(n, 2n)^{232}Pa. The ^{232}Pa ($t_{1/2}$ = 1.32 d) then beta-decays to produce ^{232}U and its progeny. This includes ^{208}Tl ($t_{1/2}$ = 3.05 m) which has a high-energy gamma-emission of 2614.5 keV resulting in high dose exposure rates and additional gamma-spectrometry interferences [19]. The X-ray and gamma-emissions from ^{233}U have low emission probabilities that make conventional NDA techniques challenging, especially when in the presence of other radionuclide interferences (Table 1).

Using the ARGO, ^{233}U assay is achievable using each detector individually, or through combining measurements to produce a sum spectrum. This more sensitive dual-detector approach provides a near 4π geometry and effectively doubles the detection efficiency. Using dual detectors also enables Compton suppressed anticoincidence spectra, whereby coincident events between both detectors (including Compton scattered events) are rejected. This provides a reduction in the Compton continuum (depending on sample composition and geometry up to 6.5% has been demonstrated) and a suppression of radionuclides that emit multiple gamma photons simultaneously (e.g., ^{132}I by 32.0% and ^{140}La by 23.4%). Sensitivity is further enhanced through the dual-detector measurement of radionuclides that emit two or more gamma-rays in cascade. Although detection efficiency is reduced using this configuration, selection of coincident gamma-energies significantly reduces the background by a factor of up to 10^6 [17]. Due to the relatively complicated nuclear decay scheme for ^{233}U, there are over 794 coincidence combinations that have potential to be measured in this manner (Fig. 1). For many combinations the coincidence probability is very low, or there are multiple gamma-emissions in coincidence, such that they are not practical for direct measurement. Identifying the most detectable signatures based upon their probability of detection and measurement efficiency was performed using a Monte Carlo approach that utilizes the Evaluated Nuclear Structure Data File (ENSDF) for radionuclides of interest.

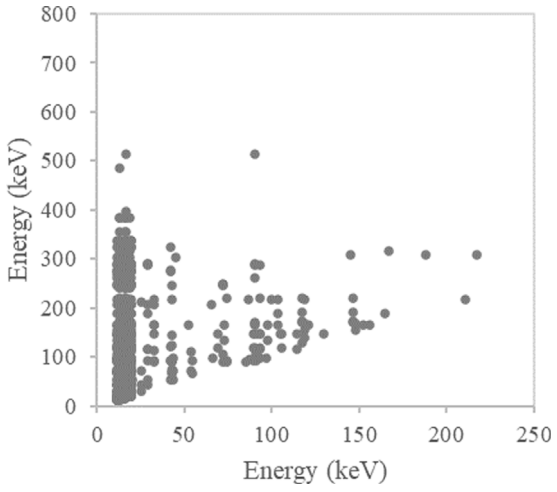

Fig. 1. Coincidence gamma-ray emissions of ^{233}U. Note most coincident gamma-rays occur at low energies where Compton scattering is highest.

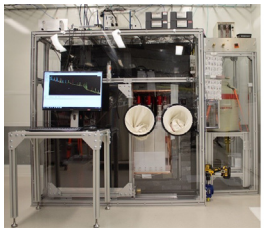

Fig. 2. Photographs of the ARGO, showing the entire system with the measurement chamber door open (left) and the dual BEGe detectors surrounded by additional NaI detectors that were removed for this work (right).

3. Methodology

3.1. The ARGO

The ARGO includes two ultra-low background Canberra BEGe detectors (model BE5030) made with high-purity copper cryostats (Fig. 2). The detectors were designed for an up–down configuration, with up-looking and down-looking U-style cryostats. Each detector has a 0.6 mm carbon epoxy window (for transmission below 10 keV) and a germanium crystal with an active area of 5000 mm^2. High voltage was set at +4500 V with a rise time of 5.6 μs and flat top of 0.8 μs. The BEGe detectors were situated within a low-background graded shield of lead (200 mm), 30% borated polyethylene (12.5 mm), cadmium (1 mm), lead (50 mm), tin (1 mm) and copper (1 mm) and the 'air gap' flushed with nitrogen gas for removal of radon isotopes. The lead was from the Doe Run lead plant (the last lead plant to close in the USA) and assayed to contain 30.2 ± 0.6 Bq kg^{-1} ^{210}Pb, < 16 μBq kg^{-1} ^{238}U and 1.7 ± 0.1 μBq kg^{-1} ^{232}Th [21]. Twelve additional sodium iodide (NaI) detectors also surround the BEGe detectors [11] but were removed to reduce the complexity of processing the TLIST data. Surrounding the shield were six Eljen Technology polyvinyltoluene (PVT) plastic scintillation plates each fitted with two ET Enterprise photomultipliers (PMTs, model 9102B) to provide a cosmic veto system [22–24]. The plates were 5 cm thickness and covered all sides of the lead cave with slots to accommodate the BEGe cryostats. The PMTs were operated at + 900 V, with a rise time of 1.2 μs and flat top of 0.6 μs and connected to a Scionix 12-way power supply splitter with integrated pre-amplifier (two model AM100(6–1)–E2-X). Each BEGe detector and the combined signal of the PVT plates were connected to a Canberra Lynx MCA. The Lynx MCAs were connected using a synchronization cable to provide a continual logic pulse for clock synchronization every 1 μs [12]. The ARGO background is reduced further by operation within the Class 1000 clean counting room inside the SUL [25]. The laboratory has a calculated shielding equivalent of 30 metres of water equivalent (mwe),

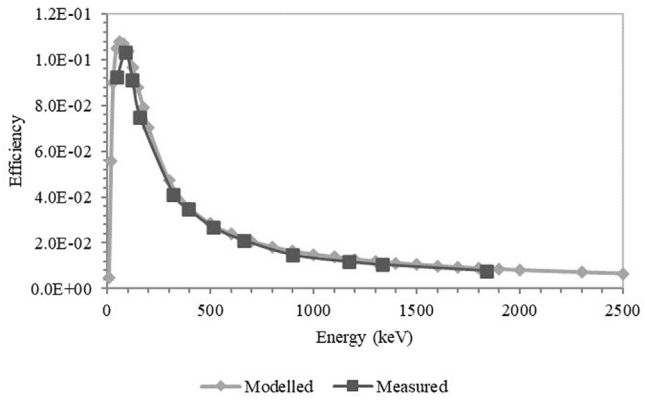

Fig. 3. Modelled and measured efficiency for the sample geometry.

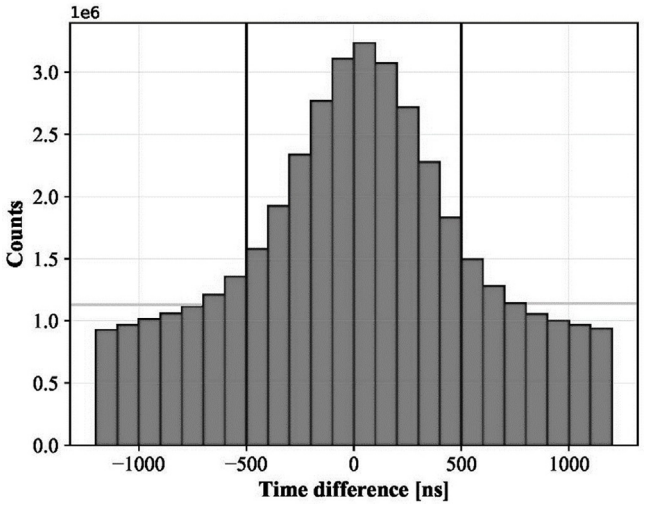

Fig. 4. The coincidence timing distribution for the ^{233}U sample (long count). The coincidence timing window is denoted by the solid vertical black lines. Beneath the horizontal grey line is predominantly random scatter.

which results in approximately 100 times fewer fast neutrons and 6 times fewer muons.

3.2. Calibration

Measurements were performed in a close geometry to maximize geometric efficiency and reduce the effects of angular correlation. This involved a perfluoroalkoxy (PFA) Savillex stability vial containing 10 ml of solution being placed between the up-looker and down-looker BEGe detectors of the ARGO system. To quantify the radionuclides from the singles and combined spectra, a mixed gamma-radiation calibration source containing the isotopes ^{210}Pb (46.5 keV), ^{109}Cd (88.0 keV), ^{57}Co (122.1 keV), ^{123m}Te (159.0 keV), ^{51}Cr (320.1 keV), ^{113}Sn (391.7 keV), ^{85}Sr (514.0 keV), ^{137}Cs (661.6 keV), ^{88}Y (898.0 keV and 1836.0 keV) and ^{60}Co (1173.2 keV and 1332.5 keV) was measured. This was also used to validate a geometry model of the Savillex stability vial using the Canberra In Situ Object Counting Systems (ISOCS) calibration software [26]. Both the modelled and measured efficiency were shown to be in excellent agreement (Fig. 3). The same model was then used to calculate true coincidence summing (TCS) and peak-to-total corrections. All nuclear data was from the Evaluated Nuclear Data File (ENDF VIII.0) database hosted by Brookhaven National Laboratory [20].

Table 2
Sample count information. An additional longer (*) count was performed to demonstrate coincidence measurements of ^{233}U.

Sample	^{233}U mass (mg)	Live time (s)	Dead time (%)
^{233}U	3.95	3230, 198126*	10.3
^{233}U + KCl	3.93	806	10.4
^{233}U + NaCl	3.92	844	9.8

3.3. Fuel salt samples

The feasibility of direct ^{233}U measurement was tested using a ^{233}U sample (prepared as a nitrate salt) irradiated at the Washington State University Reactor (WSUR, USA). Irradiation was performed for a duration of 3 h at 500 kW, at a thermal neutron flux (1.03×10^{12} n/cm^2/s at 0.1 meV–0.550 eV, 1.64×10^{11} n/cm^2/s at 0.550 eV–110.0 keV, 1.45×10^{12} n/cm^2/s at 110.0 keV–1.0 MeV, 8.89×10^{10} n/cm^2/s at 1.0 MeV–20.0 MeV). The sample was cooled for 12 h to reduce the short-lived activity and facilitate handling before dissolution in 3 M nitric acid. Afterwards 1.4×10^8 fissions were added to 1.4×10^6 Bq of non-irradiated ^{233}U and approximately 70 Bq of ^{232}U (to simulate ^{232}U build-up during MSR operation). Three samples were prepared in this manner, with each containing approximately 4 mg of ^{233}U. During the same irradiation, samples of KCl (99.1% purity) and NaCl (99.999% purity) were also irradiated and afterwards dissolved in 1 M HCl. Approximately 430 Bq of KCl and 300 Bq of NaCl were added to the second and third ^{233}U samples respectively. Each sample was then transferred to a 15 ml PFA Savillex stability vial and made up to 10 ml volume using 2% nitric acid. The vials were then double-packaged using high-density polyethylene (HPDE) for measurement on the ARGO system.

3.4. Data acquisition

Data acquisition was initiated 24 h after irradiation and performed using the TLIST functionality of the Lynx MCA, which utilizes the peak detect as the trigger and records each detector event with 100–200 ns time resolution [12]. This required the development of custom TLIST data acquisition software using the Canberra Lynx Software Development Kit (SDK, version 1.2.1). This was necessary as commercially available software does not allow TLIST acquisition using the Lynx MCA (the same is true for most other MCAs). The SDK provides a series of libraries that allow communication and control of the MCA. The libraries are compatible with the .NET, .COM, Java, python and web service languages. The python language was selected for software development. MCA communication was performed using the Transmission Control Protocol/Internet Protocol (TCP/IP), with saving of the event channel, event time, live time and real time for each detector event as ASCII variables to a comma separated value (CSV) file. Multiple acquisitions were performed with the longest being 2.3 days for investigating coincidence measurements (Table 2).

3.5. Data processing

The TLIST data was compiled using custom python software that produced single and combined spectra in the Canberra Configuration Access Method (CAM) format. This format is useful as it facilitates more complex analysis using the Canberra Genie 2000 Gamma Acquisition and Analysis software (e.g., peak deconvolution and true coincidence summing corrections). The Genie 2000 software was also used to calculate the minimum detectable activity (MDA) using the Currie formula [27] with a region of interest (ROI) of 1.25 channels full width half maximum (FWHM). The python software also extracted coincident events in both detectors, within a time window of ± 500 ns. A narrower timing window was used (typically this is set at ± 1200 ns) to minimize random scatter due to the increased sample activity (Fig. 4).

Table 3
The estimated coincidence detection probability for the most abundant ^{233}U emissions and comparisons with the RIMMER code.

Energy (keV)		Coincidence probability		
Energy 1	Energy 2	PNNL	RIMMER	Ratio
42.4	54.7	2.2E−06	4.3E−08	51.4
42.4	120.8	2.3E−08	7.4E−09	3.1
42.5	92.9	2.8E−09	4.5E−09	0.6
42.5	93.4	1.4E−07	1.8E−09	77.3
42.5	278.1	9.1E−10	9.9E−10	0.9
42.5	274.7	5.7E−10	6.0E−10	1.0
42.5	323.4	6.0E−10	5.1E−10	1.2
42.5	245.4	1.1E−08	7.5E−09	1.4
42.5	53.6	1.4E−08	4.6E−09	3.1
42.5	92.9	4.1E−09	4.5E−09	0.9
42.5	123.9	3.0E−09	3.7E−09	0.8
42.5	74.5	1.2E−08	2.5E−09	4.8
42.5	93.4	3.7E−07	1.8E−09	206.4
42.5	145.4	4.6E−09	1.3E−09	3.5
42.5	70.3	1.9E−09	8.1E−10	2.3
42.5	216.1	1.5E−09	6.6E−10	2.3
42.5	66.1	1.0E−09	6.4E−10	1.6
54.7	92.9	6.0E−07	8.7E−09	68.9
54.7	66.1	1.4E−07	1.2E−09	120.6
97.1	98.6	3.6E−10	1.2E−09	0.3
97.4	164.5	3.4E−07	3.3E−07	1.0
97.4	135.3	1.2E−07	1.0E−07	1.2
146.4	174.2	1.3E−08	1.1E−08	1.2
146.4	170.8	1.2E−08	1.1E−08	1.1
146.4	219.4	8.5E−09	8.1E−09	1.0
146.4	192.3	2.5E−09	1.7E−09	1.5

Coincidence events were then subtracted from the combined spectra to produce a Compton suppressed (anticoincidence) CAM spectra. Coincidence CAM spectra were also projected for coincidence gamma-energies of interest including 42.43 keV/42.63 keV, 54.70 keV, 97.37 keV and 146.35 keV.

3.6. Coincidence detection probability

Calculation of the coincidence detection probability is challenging and requires processing the ENSDF gamma and X-ray cascade data and calculating the probability of a given coincidence signature occurring. Various corrections must be applied, including gamma and X-ray cascade summing effects, conversion electron emission and pair production. For this a custom Monte Carlo routine was developed (full details of the code will be provided in a future publication by the author) and ran on the Deception supercomputer at PNNL (consisting of 96 AMD EPYC 7502 server microprocessors) for 10^{10} particle decay iterations. For ^{233}U, the calculation is lengthy due to the relatively low cascade probabilities, and a significant number of iterations are needed to provide confidence in the estimated coincidence detection probability (Table 3). These results were compared to estimates made using the Randomized Iterative Monte-Carlo Model for ENSDF Records (RIMMER) code [18,28]. The results of this comparison reflect the difficulties in accurately calculating the coincidence detection probability for very low-emission cascades, with relatively poor agreement for the 42.5 keV and 54.7 keV coincidence emissions. In such instances it was assumed that the difference was attributable to the lower number of particle decay iterations undertaken by the RIMMER code (this was estimated at 10^6 to 10^8) and that the PNNL calculated values were more representative.

4. Results and discussion

4.1. Conventional gamma-spectrometry

Conventional measurements using the combined spectra of both BEGe detectors were compiled from the TLIST data for each ^{233}U sample (Fig. 5). The most abundant ^{233}U peaks represent a relatively small region of the gamma-spectrum, with energies ranging from 42.4 keV to 97.1 keV (Fig. 5). The lower-abundance 146.4 keV emission was also evaluated as this was of interest for coincidence measurements. The spectra were relatively complex, with multiple emissions from ^{233}U and its fission products, including 110–143 peaks for the shorter ^{233}U, KCl and NaCl measurements, and 234 peaks for the longer ^{233}U measurement. Despite this complexity, and relatively high sample activity (dead time ranged from 9.8% to 10.4%), accurate measurement of the 1.4×10^6 Bq of ^{233}U activity was achievable using the 97.1 keV emission (the measurement was accurate in all instances to within 5%). This included shorter duration measurements of ~800 s and samples containing activated KCl and NaCl (Table 4). For the lower energy 42.5 keV emission, the activity was underestimated at 1.2×10^6 Bq despite being relatively free from interferences at this energy (the nearest being ^{99}Mo at 40.6 keV). Similarly, the 54.7 keV emission did not provide an accurate measurement, with the activity ranging from 8.5×10^5 Bq to 1.5×10^6 Bq. At this energy, the peak was not well defined and obscured by the increased Compton continuum at lower energy. The higher energy 146.4 keV emission also overestimated the activity at 1.5×10^6 Bq (except for the long count), most likely due to multiple interferences in proximity to the peak, including ^{141}Ce (145.4 keV) and ^{131}I (147.2 keV). The uncertainty was comparable for all measurements and ranged from 4.9% and 5.2%. All measurements were significantly above the MDA (by 2–3 orders of magnitude), which ranged from 2.8×10^3 Bq to 7.4×10^4 Bq for the shorter duration measurements and 8.0×10^2 Bq to 3.5×10^3 Bq for the longer duration measurements.

In no samples was there an indication of ^{232}U at the 57.8 keV and 129.1 keV gamma-emissions due to their lower emission probabilities of 1.999×10^{-3} and 6.818×10^{-4} respectively. Notably the ^{208}Tl emission at 2614.5 keV was very detectable, but was larger than expected (~446 Bq compared to 70 Bq ^{232}U added) indicating additional ^{232}Th (a progenitor of ^{208}Tl) within the ^{233}U sample in addition to production from ^{232}U decay.

4.2. Compton suppressed gamma-spectrometry

The suppression of the Compton continuum was limited at 1.96% and did not offer significant improvements in ^{233}U detection (Table 5). The 97.1 keV emission again provided the most accurate measurement for all sample types (correct to within 5%). As before, the 42.5 keV emission underestimated the activity at 1.2×10^6 Bq, and the 54.7 keV emission activity varied, ranging from 8.4×10^5 Bq to 1.7×10^6 Bq. Notably, the 146.4 keV emission underestimated the activity for the ^{233}U long and short samples (1.2×10^6 Bq), whereas the KCl and NaCl samples were closer to the true ^{233}U activity at 1.5×10^6 and 1.4×10^6 Bq respectively. The uncertainty remained similar, ranging from 4.9% to 5.2%. The MDA was also comparable, ranging from 4.1×10^3 Bq to 7.3×10^4 Bq and 1.0×10^3 Bq to 3.1×10^3 Bq, for the respective shorter and longer duration measurements. The relatively low Compton suppression was attributed to the Savillex counting geometry, which positions the BEGe detectors at 50 mm distance from one another. This reduced the detector solid angle and the capability of the system to detect and reject Compton scattered events.

4.3. Coincidence gamma-spectrometry

The custom python software was used to project all events in coincidence with the 42.5 keV, 54.7 keV, 97.1 keV and 146.4 keV emissions with a ± 1 keV tolerance (Table 6). Few coincidence emissions calculated the 1.4×10^6 Bq ^{233}U activity correctly, with accurate detection only achievable using the (42.5 keV, 54.7 keV), (42.5 keV, 278.1 keV), (146.4 keV, 174.2 keV) and (146.4 keV, 219 keV) emissions (Fig. 6). The agreement was not improved using the RIMMER coincidence detection probabilities. These discrepancies were largely attributable to the coincidence spectra remaining complicated, with

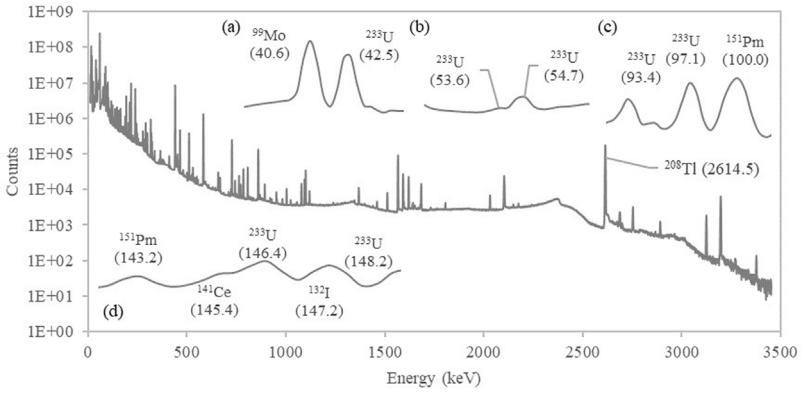

Fig. 5. Conventional gamma-spectrometry measurements of ^{233}U. The inserts show the most abundant ^{233}U peaks at (a) 42.5 keV, (b) 54.7 keV, (c) 97.1 keV and (d) 146.4 keV.

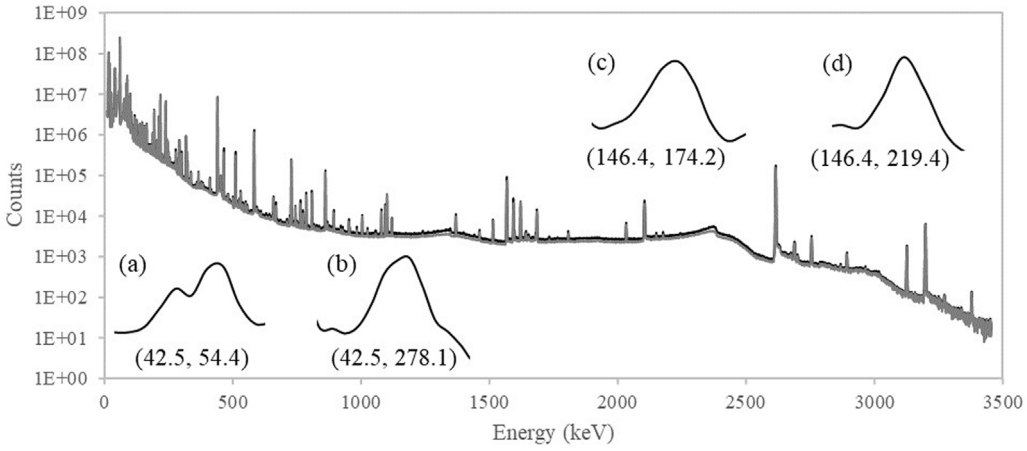

Fig. 6. Conventional (black) and Compton suppressed (grey) gamma-spectrometry measurements of ^{233}U. The inserts show the coincidence gamma-spectrometry measurements at the (a) 42.5 keV, 54.7 keV (b) 42.5 keV, 278.1 keV (c) 146.4 keV, 174.2 keV and (d) 146.4 keV, 219 keV emissions. At these energies the continuum was approximately (a) 1600, (b) 60, (c) 330 and (d) 350 counts.

Table 4
Measured ^{233}U activity for different sample types using conventional gamma-spectrometry. Each sample contained 1.4 x 10^6 Bq of ^{233}U.

Energy (keV)	Activity (Bq)			
	^{233}U long	^{233}U short	^{233}U + KCl	^{233}U + NaCl
42.5	1.2E+06 ± 6.0E+04	1.2E+06 ± 5.9E+04	1.2E+06 ± 5.7E+04	1.2E+06 ± 5.9E+04
54.7	1.5E+06 ± 7.1E+04	1.0E+06 ± 5.1E+04	1.0E+06 ± 5.2E+04	8.5E+05 ± 4.4E+04
97.1	1.4E+06 ± 7.1E+04	1.4E+06 ± 7.2E+04	1.4E+06 ± 7.0E+04	1.4E+06 ± 7.0E+04
146.4	1.4E+06 ± 6.5E+04	1.5E+06 ± 6.9E+04	1.5E+06 ± 7.2E+04	1.5E+06 ± 6.9E+04
Mean	1.4E+06 ± 1.3E+05	1.3E+06 ± 1.3E+05	1.3E+06 ± 1.3E+05	1.2E+06 ± 1.2E+05

Table 5
Measured ^{233}U activity for different sample types using Compton suppressed gamma-spectrometry. Each sample contained 1.4 × 10^6 Bq of ^{233}U.

Energy (keV)	Activity (Bq)			
	^{233}U long	^{233}U short	^{233}U + KCl	^{233}U + NaCl
42.5	1.2E+06 ± 6.1E+04	1.2E+06 ± 6.2E+04	1.2E+06 ± 5.9E+04	1.2E+06 ± 5.8E+04
54.7	1.4E+06 ± 7.0E+04	1.7E+06 ± 8.2E+04	1.0E+06 ± 5.2E+04	8.4E+05 ± 4.4E+04
97.1	1.4E+06 ± 7.1E+04	1.4E+06 ± 7.2E+04	1.4E+06 ± 7.0E+04	1.4E+06 ± 6.8E+04
146.4	1.2E+06 ± 5.4E+04	1.2E+06 ± 5.6E+04	1.5E+06 ± 7.0E+04	1.4E+06 ± 6.9E+04
Mean	1.3E+06 ± 1.3E+05	1.4E+06 ± 1.4E+05	1.3E+06 ± 1.3E+05	1.2E+06 ± 1.2E+05

multiple interfering peaks requiring deconvolution and a relatively high Compton continuum obscuring peaks of interest. These features were due to the sample activity, which resulted in significant random scattering within the 500 ns coincidence window and a breakthrough of features usually observed in the single or combined spectra (see Fig. 4). An additional effect impacted the 42.5 keV and 54.7 keV emissions, as gating on these lower energies to produce projected spectra, meant also gating on increased Compton scattered events at these energies, and introducing additional peaks that appeared in coincidence with the energy of interest. For future work, this effect could be reduced by using Compton suppressed coincidence measurements, whereby both BEGe detectors are surrounded by a Compton suppression shield to suppress scattered events from the coincidence measurement (although this significantly increases the complexity of data processing) [11]. The timing

Table 6
Coincidence measurements of ^{233}U. Measurements in bold are those in best agreement with the ^{233}U sample activity.

Energy 1	Energy 2	Probability	Activity
42.5	**54.7**	**2.2E−06**	**1.4E+04 ± 4.3E+02**
42.5	120.8	2.3E−08	2.1E+05 ± 1.1E+04
42.5	92.9	2.8E−09	6.3E+05 ± 5.5E+04
42.5	93.4	1.4E−07	5.4E+04 ± 1.0E+03
42.5	**278.1**	**9.1E−10**	**1.4E+06 ± 1.1E+05**
42.5	323.4	6.0E−10	7.4E+05 ± 1.1E+05
42.5	245.4	1.1E−08	4.6E+05 ± 1.6E+04
42.5	53.6	1.4E−08	1.2E+06 ± 7.3E+04
42.5	92.9	4.1E−09	1.1E+06 ± 9.3E+04
42.5	123.9	3.0E−09	2.2E+06 ± 8.7E+04
42.5	74.5	1.2E−08	1.2E+06 ± 3.9E+04
42.5	145.4	4.6E−09	1.1E+06 ± 5.5E+04
42.5	70.3	1.9E−09	7.7E+05 ± 3.4E+05
42.5	216.1	1.5E−09	8.5E+05 ± 9.8E+04
42.5	66.1	1.0E−09	3.2E+06 ± 5.9E+05
54.7	92.9	6.0E−07	9.9E+03 ± 8.3E+02
54.7	66.1	1.4E−07	2.7E+04 ± 2.2E+03
97.4	164.5	3.4E−07	4.2E+03 ± 8.9E+02
97.4	135.3	1.2E−07	3.1E+03 ± 3.5E+03
146.4	**174.2**	**1.3E−08**	**1.4E+06 ± 2.5E+04**
146.4	170.8	1.2E−08	2.9E+06 ± 1.3E+05
146.4	**219.4**	**8.5E−09**	**1.4E+06 ± 3.3E+04**
146.4	192.3	2.5E−09	6.2E+05 ± 1.3E+05

of the coincidence measurements was also degraded by the 10.3% dead-time resulting in a loss of some coincidence measurements. This could be largely eliminated by using detectors equipped with a transistor reset preamplifier (which has improved tolerance of high count rates and lower dead-times) instead of an RC feedback preamplifier [29].

Additional consideration should also be given to the validity of the ^{233}U nuclear data, especially given the complex decay scheme and that no previous ^{233}U coincidence measurements have been published. There exists the possibility that some refinements to the nuclear data might be required to improve the accuracy of coincidence measurements. Gamma energy and abundance differences were also noted between the ENDF (both ENDF/B-VII.1 and VIII.0) and JEFF 3.1 nuclear data archives. Future work will aim to utilize the ARGO for low-activity ^{233}U measurements with reduced dead-time and improved coincidence timing — from which further insight into the validity of the nuclear data may be obtained for coincidence measurements.

5. Conclusions

Accurate determination of ^{233}U in freshly irradiated samples is achievable using direct gamma-spectrometry techniques. This includes samples containing activated KCl and NaCl that could be considered representative of fuel salt samples from next-generation MSRs. Using the dual detector ARGO system, the four most abundant gamma-emissions were evaluated (42.5 keV, 54.7 keV, 97.1 keV, 146.4 keV), and the 97.1 keV emission consistently provided accurate measurements of the ^{233}U activity (to within 5%). This included short duration measurements (~800 s) at relatively high dead times (10.4%). Utilizing Compton suppression functionality did not offer significant improvements in ^{233}U detection, and the 97.1 keV emission again provided the most accurate measurements, although suppression was limited at only 1.96% due to the sample geometry. It was also demonstrated that ^{233}U could be determined using four of its coincidence gamma-emissions (42.5 keV, 54.7 keV; 42.5 keV, 278.1 keV; 146.4 keV, 174.2 keV; 146.4 keV, 219 keV) emissions. Measurement using other coincidence emissions is likely to be achievable but may require improvements in the coincidence timing, dead-time and potentially the nuclear data. This work has demonstrated ^{233}U determination using the ARGO laboratory system, and it is envisaged that a similar dual-detector configuration could be utilized for online safeguards measurements.

CRediT authorship contribution statement

Jonathan L. Burnett: Conceptualization, Methodology, Validation, Formal analysis, Investigation, Writing – original draft, Writing – review & editing.

Declaration of competing interest

The authors declare that they have no known competing financial interests or personal relationships that could have appeared to influence the work reported in this paper.

Acknowledgements

This research was funded by the National Nuclear Security Administration, Office of Defense Nuclear Nonproliferation Research and Development (NNSA DNN R&D), USA. Thank you to Allan Myers, James Bowen, Manish Sharma, Sean Stave and Martin Keillor at Pacific Northwest National Laboratory (USA), Ashley Davies and Richard Britton at the Atomic Weapons Establishment (UK), and Troy Anderson at Mirion Technologies (USA), for their support to this project. The views expressed here do not necessarily reflect the opinion of the United States Government or the United States Department of Energy. Pacific Northwest National Laboratory is operated for the U.S. Department of Energy by Battelle under Contract DE-AC05-76RL01830.

References

[1] E.S. Bettis, et al., The aircraft reactor experiment—Design and construction, Nucl. Sci. Eng. 2 (6) (1957) 804–825.
[2] E.S. Bettis, et al., The aircraft reactor experiment—Operation, Nucl. Sci. Eng. 2 (6) (1957) 841–853.
[3] W.K. Ergen, et al., The aircraft reactor experiment—Physics, Nucl. Sci. Eng. 2 (6) (1957) 826–840.
[4] P.N. Haubenreich, J.R. Engel, Experience with the molten-salt reactor experiment, Nucl. Appl. Technol. 8 (2) (1970) 118–136.
[5] R.C. Robertson, MSRE Design and Operations Report. Part I. Description of Reactor Design, Oak Ridge National Lab. Tenn., 1965, p. 561, Medium, ED; Size.
[6] G. Locatelli, M. Mancini, N. Todeschini, Generation IV nuclear reactors: Current status and future prospects, Energy Policy 61 (2013) 1503–1520.
[7] L.G. Worrall, et al., Safeguards considerations for thorium fuel cycles, Nucl. Technol. 194 (2) (2016) 281–293.
[8] IAEA, The Structure and Content of Agreements Between the Agency and States Required in Connection with the Treaty on the Non-Proliferation of Nuclear Weapons, International Atomic Energy Agency, Vienna, Austria, 1972.
[9] IAEA, The Physical Protection of Nuclear Material, International Atomic Energy Agency, Vienna, Austria, 2011.
[10] J.L. Burnett, et al., Development of a multidimensional gamma-spectrometer, J. Radioanal. Nucl. Chem. (2017) 1–6.
[11] A.V. Davies, J.L. Burnett, R. Britton, Performance testing of a compton suppressed coincidence measurements using the advanced radionuclide Gamma-spectrometer, Nucl. Instrum. Methods Phys. Res. A 951 (2020) 163009.
[12] J.L. Burnett, A.V. Davies, Investigating the time resolution of a compact multidimensional gamma-spectrometer, J. Radioanal. Nucl. Chem. 288 (3) (2011) 699–703.
[13] R. Britton, et al., Monte-Carlo optimisation of a compton suppression system for use with a broad-energy HPGe detector, Nucl. Instrum. Methods Phys. Res. A. 762 (2014) 42–53.
[14] R. Britton, et al., Monte Carlo characterisation of a compton suppressed broad-energy HPGe detector, J. Radioanal. Nucl. Chem. 300 (3) (2014) 1253–1259.
[15] J.L. Burnett, A.V. Davies, Compton suppressed gamma-spectrometry for comprehensive nuclear-test-ban treaty samples, J. Radioanal. Nucl. Chem. 295 (1) (2013) 497–499.
[16] R. Britton, et al., Coincidence corrections for a multi-detector gamma spectrometer, Nucl. Instrum. Methods Phys. Res. A. 769 (2015) 20–25.
[17] R. Britton, et al., A high-efficiency HPGe coincidence system for environmental analysis, J. Environ. Radioact. 146 (2015) 1–5.
[18] R. Britton, M.J. Jackson, A.V. Davies, Quantifying radionuclide signatures from a γ–γ coincidence system, J. Environ. Radioact. 149 (2015) 158–163.
[19] M.H. Haghighi, et al., In situ NDA conformation measurements performed at auxiliary charcoal bed and other main charcoal beds after uranium removal from molten salt reactor experiment ACB at Oak Ridge national laboratory, in: Waste Management 2002 Symposium, United States, 2002.

[20] NNDC, Evaluated Nuclear Data File (ENDF), National Nuclear Data Center (NNDC), Brookhaven National Laboratory, USA, 2018.
[21] J.L. Orrell, et al., Assay methods for 238U, 232Th, and 210Pb in lead and calibration of 210Bi bremsstrahlung emission from lead, J. Radioanal. Nucl. Chem. 309 (3) (2016) 1271–1281.
[22] J.L. Burnett, A.V. Davies, Cosmic veto gamma-spectrometry for comprehensive nuclear-test-ban treaty samples, Nucl. Instrum. Methods Phys. Res. A. 747 (2014) 37–40.
[23] J.L. Burnett, A.V. Davies, Development of a cosmic veto gamma-spectrometer, J. Radioanal. Nucl. Chem. 291 (3) (2012) 1007–1010.
[24] J.L. Burnett, A.V. Davies, J.L. McLarty, Further development of a cosmic veto gamma-spectrometer, J. Radioanal. Nucl. Chem. 298 (2) (2013) 987–992.
[25] C.E. Aalseth, et al., A shallow underground laboratory for low-background radiation measurements and materials development, Rev. Sci. Instrum. 83 (11) (2012) 113503.
[26] R. Venkataraman, et al., Validation of in situ object counting system (ISOCS) mathematical efficiency calibration software, Nucl. Instrum. Methods Phys. Res. A 422 (1) (1999) 450–454.
[27] L.A. Currie, Limits for qualitative detection and quantitative determination. Application to radiochemistry, Anal. Chem. 40 (3) (1968) 586–593.
[28] R. Britton, M.J. Jackson, A.V. Davies, Incorporating X–ray summing into gamma–gamma signature quantification, Appl. Radiat. Isot. 116 (2016) 128–133.
[29] J.K. Zickefoose, et al., Spectroscopic noble gas stack monitor with continuous unattended operation and analysis, J. Radioanal. Nucl. Chem. 318 (1) (2018) 387–393.